Geophysical Prospecting, 2002, **50**, 629–643

Wavefield extrapolation and prestack depth migration in anelastic inhomogeneous media

Jianfeng Zhang† and Kees Wapenaar*

Centre for Technical Geoscience, Delft University of Technology, PO Box 5028, 2600 GA Delft, The Netherlands

Received December 2001, revision accepted July 2002

ABSTRACT

Wavefield depth extrapolation and prestack depth migration in complex anelastic media are studied. Kjartansson's frequency-independent Q law is used to describe the absorption of seismic energy. The macromodel used is analogous to the macromodel used for current migration schemes except that an additional frequency-independent Q macromodel needs to be provided. Absorption in the forward one-way propagator is introduced by assuming a complex phase velocity, and the inverse one-way propagator is obtained using the reciprocity theorem for one-way wavefields in dissipative media. The stability of the inverse propagator is achieved by limiting the angle of propagation of wavefields. A table-driven explicit operator scheme for imaging complex 2D anelastic media is presented. High-accuracy, short convolution operators are designed by the weighted least-squares method, and two kinds of imaging conditions are proposed. Numerical examples of depth extrapolation in laterally varying media, the migration of a spatial impulse with dispersion as well as shot record depth migration demonstrate the potential of the proposed explicit forward operator, the explicit inverse operator and the prestack depth migration scheme, respectively.

INTRODUCTION

Anelasticity of a medium will cause dissipation of seismic energy, thus decreasing the amplitude and modifying the phase. This attenuation and dispersion of the seismic wave requires suitable treatment for imaging the reflectivity of the subsurface with better resolution. The first attempts to treat dissipation were directed towards the elimination of its effects from the measured data by so-called inverse Q-filters (Robinson 1979). Since the effects of dissipation increase with the length of the wave path, the filters are time variant. Rather than compensating for the effects of absorption in a separate preprocessing step, it is more accurate and efficient to do this during the imaging itself. This approach was followed by Mittet, Sollie and Hokstad (1995) for explicit prestack migration and by Causse and Ursin (2000) for reverse-time migration. Moreover, the absorption effects have been incorporated into seismic wave modelling (Emmerich and Korn 1987; Carcione, Kosloff and Kosloff 1988; Stekl and Pratt 1998) and inversion (Keers, Vasco and Johnson 2001).

In seismic migration, images of the subsurface are commonly obtained by eliminating the propagation effects from the seismic measurements. For anelastic media, the attenuation and dispersion of the seismic wave due to intrinsic absorption should be included in this elimination of propagation effects. Hence, for prestack depth migration in anelastic media it is necessary to develop a forward wavefield depth extrapolation scheme that can model the attenuation and dispersion and an inverse extrapolation scheme that can compensate this attenuation and dispersion. Since the anelastic stress–strain relationship involves time integration in the wave equation in the time domain, frequency-domain algorithms, which can incorporate arbitrary absorption laws, are a

*E-mail: C.P.A.Wapenaar@ctg.tudelft.nl
†On leave from Department of Engineering Mechanics, Dalian University of Technology, Dalian 116023, China.

© 2002 European Association of Geoscientists & Engineers

good alternative to reverse-time extrapolation and other time-domain migration schemes. For the frequency-domain algorithms, the absorption in the forward one-way propagator in inhomogeneous media may be introduced by allowing for a complex phase velocity, and the inverse one-way propagator is obtained using the reciprocity theorem for one-way wavefields in inhomogeneous dissipative media (Wapenaar, Dillen and Fokkema 2001). Stability is achieved by suppressing a part of the eigenvalue spectrum of the square-root operator for the adjoint version of the dissipative medium, which means that we have to limit the angle of propagation of the wavefields. The explicit extrapolation operator has proved its effectiveness in imaging steeply dipping reflectors in the presence of lateral velocity variations for lossless media (Holberg 1988; Hale 1991; Zhang, Verschuur and Wapenaar 2001). This space–frequency domain scheme also provides a good approximation for constructing the one-way forward and inverse propagators in an inhomogeneous dissipative medium. The maximum angle of propagation can be controlled in the design of the spatial convolution operators for the explicit operator scheme. Thus it becomes efficient to suppress a part of the eigenvalue spectrum of the corresponding square-root operator numerically with this scheme. Furthermore, the explicit scheme requires the absorption effects to be included only in the design of the convolution operators so that the resulting operator can easily be incorporated in existing migration schemes. Hence, we adapt the explicit extrapolation operator scheme to accommodate absorption for performing forward and inverse wavefield extrapolation in anelastic inhomogeneous media and imaging complex anelastic structures. Here, the short spatial convolution operators are designed by adapting the weighted least-squares method (Thorbecke and Rietveld 1994), which can derive a highly accurate short operator at a very low computational cost.

The proposed explicit operator scheme can be applied in general and can accommodate any frequency-dependent or frequency-independent absorption laws. However, from the point of view of seismic exploration, it is more practical to obtain a macromodel that is described by a real phase velocity, as in lossless media, and an additional frequency-independent quality factor Q. We use Kjartansson's (1979) frequency-independent Q law in our wavefield extrapolation and prestack depth migration scheme. Thus the macromodel we use is more realistic and is closely related to the macromodel used for current migration schemes, except that an additional Q macromodel must be provided. The Q macromodel may be estimated, e.g. from VSP data as suggested by Amundsen and Mittet (1994). The proposed scheme is implemented by first precalculating an operator table using real phase velocities at a chosen reference frequency and quality factor Q, and then selecting the appropriate convolution operators according to the macromodel during the depth extrapolation.

A synthetic seismic experiment is designed to test the proposed prestack migration scheme. The data set is generated by a frequency-domain finite-difference method. The accuracy of the proposed explicit depth extrapolation scheme is demonstrated by comparing the results of the explicit depth extrapolation with modelled seismograms using the frequency-domain finite-difference method in laterally varying viscoacoustic media. The performance of the derived short convolution operators for anelastic media is illustrated by computing migration impulse responses of a Ricker wavelet with dispersion. The comparison of the impulse responses with and without compensation for absorption also demonstrates the satisfactory compensation for dispersion by the proposed explicit scheme.

FREQUENCY-INDEPENDENT Q LAW

In the frequency domain, it is common to account for absorption by assuming a complex, frequency-dependent bulk modulus $M(\omega)$, and then the quality factor Q is defined as

$$Q(\omega) = \mathrm{Re}M(\omega)/\mathrm{Im}M(\omega). \tag{1}$$

The real and imaginary parts of $M(\omega)$ must obey a Kramers–Kronig relationship (Aki and Richards 1980). In seismic applications, Q is often assumed to be either frequency-independent or only slowly varying with frequency. However, from a practical point of view of the estimation of a macromodel for seismic migration, the choice of a frequency-independent Q is very effective. For a frequency-independent Q, the bulk modulus is given by (Kjartansson 1979)

$$M(\omega) = |M(\omega_\mathrm{r})|(\mathrm{j}\omega/\omega_\mathrm{r})^{(2/\pi)\arctan Q^{-1}}, \tag{2}$$

where ω_r is an arbitrarily chosen reference (angular) frequency and j is the imaginary unit. For a homogeneous attenuating plane wave, based on the viscoacoustic wave equation, the real phase velocity can be expressed as (Aki and Richard 1980, equation (5.96))

$$c_0(\omega) = \left(\frac{\mathrm{Re}M}{\rho}\right)^{1/2}\left(\frac{2(1+Q^{-2})}{1+\sqrt{1+Q^{-2}}}\right)^{1/2}. \tag{3}$$

From (2) and (3), the complex phase velocity is obtained as

$$c^2(\omega) = \frac{1}{2}\left(1 + \frac{1}{\sqrt{1+Q^{-2}}}\right) c_0^2(\omega_r)(\mathrm{j}\omega/\omega_r)^{(2/\pi)\arctan Q^{-1}}. \quad (4)$$

Thus we can use Q and the real phase velocity at a reference frequency to determine uniquely the frequency-dependent complex phase velocities. By contrast, a standard linear solid theory that has a strongly frequency-dependent Q was used by Mittet *et al.* (1995).

FORWARD AND INVERSE ONE-WAY WAVEFIELD PROPAGATORS

In the space–frequency domain ($\mathbf{x}$,ω), the viscoacoustic wave equation in an inhomogeneous dissipative medium, in the absence of sources, can be expressed for the pressure $P(\mathbf{x},\omega)$ as follows:

$$\rho\nabla\cdot\left(\frac{1}{\rho}\nabla P\right) + \frac{\omega^2}{c^2(\mathbf{x},\omega)}P = 0, \quad (5)$$

where $c(\mathbf{x},\omega)$ is the complex phase velocity, $\rho(\mathbf{x})$ is the density, and $\mathbf{x}=(x,y,z)$ is the Cartesian coordinate vector; the z-axis points vertically downwards. We divide the inhomogeneous medium into thin horizontal layers according to the vertical variation of the medium parameters, and we assume that the medium parameters are independent of z in each thin layer. Next we discuss one-way wavefield propagators for a vertically invariant layer with its upper horizontal surface defined as Σ_0 at $z=z_0$ and its lower horizontal surface defined as Σ_1 at $z=z_1$. Following Wapenaar and Berkhout (1989), we can derive the one-way wave equation from (5) in this vertically invariant layer as

$$\partial_z P^{\pm}(\mathbf{x},\omega) = \mp\mathrm{j}\hat{H}_1 P^{\pm}(\mathbf{x},\omega), \quad (6)$$

where $P^+(\mathbf{x},\omega)$ and $P^-(\mathbf{x},\omega)$ are the one-way wavefields that propagate in the positive and negative z-directions, respectively, and $\hat{H}_1$ is the so-called square-root operator. The square-root operator is related to the Helmholtz operator $\hat{H}_2$, as follows:

$$\hat{H}_2 = \hat{H}_1\hat{H}_1. \quad (7)$$

In a 2D configuration, the velocity and density in the thin layer are now given by $c=c(x,\omega)$ and $\rho=\rho(x)$ and the Cartesian coordinate vector reduces to $\mathbf{x}=(x,z)$. The Helmholtz operator may then be written as

$$\hat{H}_2 = \frac{\omega^2}{c^2(x,\omega)} - \frac{3(\partial_x\rho)^2}{4\rho^2} + \frac{\partial_x^2\rho}{2\rho} + \partial_x^2. \quad (8)$$

Here, we use the one-way reciprocity theorem to derive the inverse wavefield propagator. For this purpose, it is useful to introduce an adjoint (effective) version of the dissipative medium. The bulk modulus for the effective medium is defined as

$$M'(x,\omega) = \{M(x,\omega)\}^*, \quad (9)$$

where the superscript * denotes the complex conjugate. Effective media are usually associated with a computational state. When the medium in one state is the adjoint effective version of the dissipative medium in the other state, the correlation type reciprocity theorem for one-way wavefields in dissipative media can be reduced to (Wapenaar *et al.* 2001)

$$\int_{\partial D}\{(P_A^+)^* P_B^+ - (P_A^-)^* P_B^-\} n_z \mathrm{d}x = \int_D \{(P_A^+)^* S_B^+ - (P_A^-)^* S_B^- + (S_A^+)^* P_B^+ - (S_A^-)^* P_B^-\}\mathrm{d}\mathbf{x}, \quad (10)$$

where $\partial D = \Sigma_0 \cup \Sigma_1$ is the surface enclosing the domain D occupied by the thin layer, n_z is the component in the z-direction of the outward pointing normal vector to ∂D with $n_z=-1$ for $z=z_0$ and $n_z=+1$ for $z=z_1$, and $S_A^{\pm}$ and $S_B^{\pm}$ are, respectively, one-way sources for the two states. The subscripts B and A refer to the actual dissipative medium and the adjoint (effective) version of the dissipative medium, respectively.

Consider sources $S_A^+ = \delta(\mathbf{x}-\mathbf{x}')$, $S_A^- = 0$, $S_B^+ = \delta(\mathbf{x}-\mathbf{x}'')$ and $S_B^- = 0$ for the two states, respectively. If we choose $\mathbf{x}'$ and $\mathbf{x}''$ such that both are outside D, (10) can be rewritten as

$$\int_{\Sigma_1}\{(P_A^+)^* P_B^+ - (P_A^-)^* P_B^-\}\mathrm{d}x = \int_{\Sigma_0}\{(P_A^+)^* P_B^+ - (P_A^-)^* P_B^-\}\mathrm{d}x. \quad (11)$$

Let $\mathbf{x}'$ and $\mathbf{x}''$ be positioned at the horizontal surface Σ_0^-, where Σ_0^- lies just above Σ_0 (it is defined by $z_0^- = z_0 - \varepsilon$, where ε is a vanishing positive constant). We then have

$$\begin{matrix} P_A^+(\mathbf{x},\mathbf{x}') = \delta(\mathbf{x}-\mathbf{x}'), & P_A^-(\mathbf{x},\mathbf{x}') = 0, \\ P_B^+(\mathbf{x},\mathbf{x}'') = \delta(\mathbf{x}-\mathbf{x}''), & P_B^-(\mathbf{x},\mathbf{x}'') = 0, \end{matrix} \quad \mathbf{x}\subset\Sigma_0, \quad (12a)$$

$$\begin{matrix} P_A^+(\mathbf{x},\mathbf{x}') = W_A^+(\mathbf{x},\mathbf{x}'), & P_A^-(\mathbf{x},\mathbf{x}') = 0, \\ P_B^+(\mathbf{x},\mathbf{x}'') = W_B^+(\mathbf{x},\mathbf{x}''), & P_B^-(\mathbf{x},\mathbf{x}'') = 0, \end{matrix} \quad \mathbf{x}\subset\Sigma_1, \quad (12b)$$

where $W_A^+(\mathbf{x},\mathbf{x}')$ and $W_B^+(\mathbf{x},\mathbf{x}'')$ denote the forward propagators for downgoing waves, i.e. the Green's functions of the one-way wave equation (6) for the two states. Substituting (12) into (11) leads to

$$\int_{\Sigma_1}\{W_A^+(\mathbf{x},\mathbf{x}')\}^* W_B^+(\mathbf{x},\mathbf{x}'')\mathrm{d}x = \delta(\mathbf{x}'-\mathbf{x}''). \quad (13)$$

From (13), the inverse propagator $F_{\mathrm{B}}^{+}(\mathbf{x}',\mathbf{x})$ for downgoing waves in the dissipative medium (state B) can be expressed as

$$F_{\mathrm{B}}^{+}(\mathbf{x}',\mathbf{x}) = \{W_{\mathrm{A}}^{+}(\mathbf{x},\mathbf{x}')\}^{*}, \tag{14}$$

where $W_{\mathrm{A}}^{+}(\mathbf{x},\mathbf{x}')$ is the forward propagator in the adjoint (effective) medium. From reciprocity we also have

$$F_{\mathrm{B}}^{+}(\mathbf{x}',\mathbf{x}) = F_{\mathrm{B}}^{-}(\mathbf{x},\mathbf{x}'), \quad W_{\mathrm{A}}^{+}(\mathbf{x},\mathbf{x}') = W_{\mathrm{A}}^{-}(\mathbf{x}',\mathbf{x}), \tag{15}$$

and thus the inverse (downward continuation) propagator for upgoing waves is obtained as

$$F_{\mathrm{B}}^{-}(\mathbf{x},\mathbf{x}') = \{W_{\mathrm{A}}^{-}(\mathbf{x}',\mathbf{x})\}^{*}. \tag{16}$$

Equations (14) and (16) show that the inverse propagators in a dissipative medium are expressed as the complex conjugate of the forward propagators in the adjoint (effective) medium. For prestack migration in a dissipative medium, downward extrapolation of the upgoing receiver wavefield should be performed with the inverse propagator $F_{\mathrm{B}}^{-}(\mathbf{x},\mathbf{x}')$ for the dissipative medium. Downward extrapolation of the downgoing source wavefield could be performed either with the forward propagator $W_{\mathrm{B}}^{+}(\mathbf{x},\mathbf{x}')$ in the dissipative medium or with $W_{\mathrm{A}}^{+}(\mathbf{x},\mathbf{x}')$ in the effective medium, depending on the choice of imaging condition, see (19) and (20) below.

For lossless, laterally varying media, Grimbergen, Dessing and Wapenaar (1998) constructed expressions for $W^{\pm}$ in terms of eigenvalues and eigenfunctions of the self-adjoint Helmholtz operator. For arbitrary laterally varying layers, these eigenvalues and eigenfunctions were obtained numerically. A similar approach could be followed for dissipative laterally varying media. However, because the theory for operators that are not self-adjoint has many pitfalls and because the numerical solution of eigenvalues and eigenfunctions is expensive, we introduce instead an approximate solution in the next section. We conclude this section by considering the special case of a dissipative laterally invariant medium. For this situation we can solve the forward propagators for the two states from (6) for $\omega > 0$ as

$$W_{\mathrm{B}}^{+}(x,z_1;x',z_0) = \int \exp(\mathrm{j}k_x x)\exp\{-\mathrm{j}(z_1-z_0)\sqrt{\lambda_{\mathrm{B}}(k_x)}\}\exp(-\mathrm{j}k_x x')\mathrm{d}k_x, \quad \mathrm{Im}\left(\sqrt{\lambda_{\mathrm{B}}(k_x)}\right) < 0 \tag{17a}$$

$$W_{\mathrm{A}}^{-}(x',z_0;x,z_1) = \int \exp(\mathrm{j}k_x x)\exp\{\mathrm{j}(z_0-z_1)\sqrt{\lambda_{\mathrm{A}}(k_x)}\}\exp(-\mathrm{j}k_x x')\mathrm{d}k_x, \quad \mathrm{Im}\left(\sqrt{\lambda_{\mathrm{A}}(k_x)}\right) > 0 \tag{17b}$$

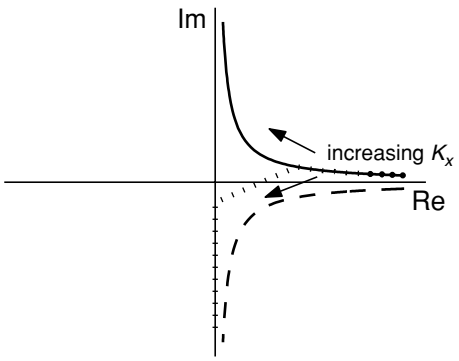

Figure 1 Example of eigenvalue spectra (in the complex plane) of the square-root operator for a dissipative medium ($\sqrt{\lambda_{\mathrm{B}}(k_x)}$) and its adjoint effective version ($\sqrt{\lambda_{\mathrm{A}}(k_x)}$). The dashed line denotes the dissipative medium, the solid line denotes the effective medium, and the dotted line denotes the modified eigenvalue spectrum of the effective medium.

where $\lambda_{\mathrm{B}}(k_x)$ and $\lambda_{\mathrm{A}}(k_x)$ are, respectively, eigenvalue spectra of the Helmholtz operator for a dissipative medium and its adjoint effective version, given by

$$\lambda_{\mathrm{B}}(k_x) = \omega^2/c^2(\omega) - k_x^2, \quad \lambda_{\mathrm{A}}(k_x) = \omega^2/\{c^2(\omega)\}^{*} - k_x^2, \tag{18}$$

where $c(\omega)$ is the complex phase velocity as expressed in (4). The square roots of the eigenvalue spectra (i.e. the eigenvalue spectra of the square-root operator) are illustrated in Fig. 1. It can be seen that W_{A}^{-} tends to infinity, as does F_{B}^{-}, when $|k_x|$ is large. This shows the instability of the inverse propagator in the dissipative medium. For stabilization, we need to suppress the eigenvalue spectrum for $|k_x|$ exceeding a given frequency-dependent k_c. After this suppression, we get a new eigenvalue spectrum for the corresponding square-root operator shown by the dotted line in Fig. 1. We can thus obtain a modified inverse propagator $\bar{F}_{\mathrm{B}}^{-}$, which is conditionally stable for a finite number of extrapolation steps.

EXPLICIT DEPTH EXTRAPOLATION

The explicit extrapolation operator scheme provides an approximation to determine the forward and inverse propagators in a laterally varying medium. The assumption is made that the medium is homogeneous within the spatial extent of the propagator. Thus we can derive a local propagator from (17) as in a laterally invariant medium, with the medium parameters equal to the values at the central gridpoint of the aperture of the propagator, and we let that specific propagator be used only for that gridpoint. For other gridpoints, the propagator is obtained using the corresponding medium

parameters. Thus we can obtain approximate solutions for the propagators at all gridpoints for the laterally varying medium. The experience in lossless media has proved the effectiveness (Holberg 1988) and limitations (Etgen 1994) of this approximation.

By reducing the spatial extent of the propagator, we gain the following: (i) the computational cost of the spatial convolution during the depth extrapolation is reduced; (ii) the assumption we made becomes more acceptable. Hence, for an explicit extrapolation operator scheme, it is necessary to design a short convolution operator in the space–frequency domain such that its spatial Fourier transform matches $\exp\{-j\Delta z\sqrt{\lambda_B(k_x)}\}$ or $\exp\{-j\Delta z\sqrt{\lambda_A(k_x)}\}$ as accurately as possible for $|k_x|$ less than a given value k_c and that its amplitudes decay for k_x outside this range.

Different design methods exist for short operators (Holberg 1988; Hale 1991; Soubaras 1996). Mittet *et al.* (1995) used Holberg's (1988) non-linear least-squares method to design short convolution operators. However, this method has a high computational cost, whereas Hale's (1991) Taylor series expansion method is more efficient but less accurate (in the latter method, the errors are unnecessarily small for small wavenumbers and grow rapidly with increasing wavenumbers). The weighted least-squares method (Thorbecke and Rietveld 1994), although without constraints on the amplitudes, can be used to derive a stable, highly accurate 1D convolution operator at a very low computational cost in a lossless medium. Here, we adapt the weighted least-squares method to design short convolution operators for dissipative media. Since the amplitude of the inverse operator in dissipative media should exceed 1.0 and its magnitude increases as the angle of propagation increases, we must first determine a maximum angle of propagation in order to guarantee that application of the operators will magnify amplitudes by no more than an accepted maximum magnitude. This means that the proposed scheme puts a limitation on the migration dip. For real data, the maximum angle of propagation is determined, based on the maximum frequency of the data, the magnitude of Q and its distribution in the macromodel, the approximated number of extrapolation steps and the accepted maximum magnitude. Based on the maximum angle of propagation, we can determine the value of k_c (for suppressing the eigenvalue spectra) at each frequency and define the weight to be a very small value (e.g. 10^{-5}) for $|k_x| > k_c$. Moreover, we change the spectrum of the exact propagators for $|k_x| > k_c$ to a smooth function that decays to zero. Thus we can derive a conditionally stable, highly accurate short operator in dissipative media by the weighted least-squares method. Figure 2 shows an amplitude spectrum in the wavenumber domain for a 25-point explicit inverse operator, where $\Delta z = 12$ m, $\omega/2\pi = 29$ Hz, $\omega_r/2\pi = 25$ Hz, $c_0(\omega_r) = 2000$ m/s, $Q = 50$, and we assume the accepted maximum amplitude of the operator is 1.03. Thus k_c is obtained as 0.08 (here $\Delta x = 30.0$), which is related to a maximum angle of propagation of 60°. From Fig. 2 we find that the derived explicit inverse operator matches the exact inverse operator well in the range bounded by the maximum angle of propagation. Furthermore, the comparison of the amplitude spectrum of the exact inverse operator with the derived short operator illustrates the stabilizing effect of the proposed scheme. It should be noted that the fact that the maximum amplitude of the derived operator does not approach 1.03 in Fig. 2 is due to the fact that the frequency corresponding to this operator is $0.77\omega_{max}$ instead of ω_{max}. Figure 3 shows further the difference between the phase spectra for dissipative and lossless media for the exact inverse operators, where the

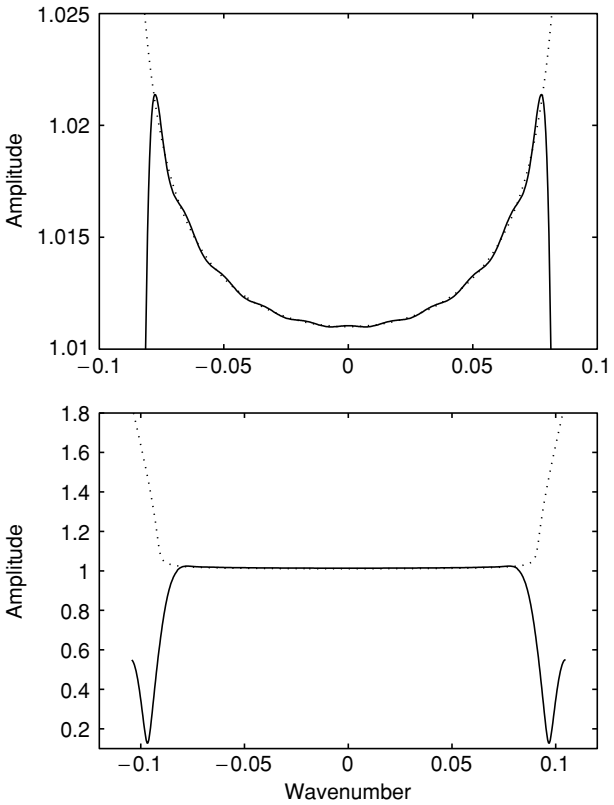

Figure 2 Amplitude spectrum for a derived 25-point explicit inverse operator (solid lines). The dotted lines represent the spectrum of the exact inverse extrapolation operator. The top figure shows a detailed view around 1.015. The quality factor related to the operator is 50.

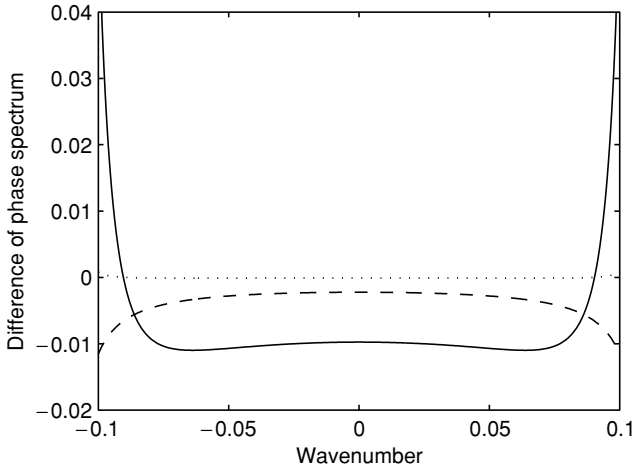

Figure 3 The difference between the phase spectra for the dissipative and lossless media for the exact inverse operators. The solid line denotes the case of $\omega/2\pi = \omega_r/2\pi = 35$ Hz and $Q = 5$, the dotted line denotes the case of $\omega/2\pi = \omega_r/2\pi = 35$ Hz and $Q = 50$, and the dashed line denotes the case of $\omega/2\pi = 35$ Hz, $\omega_r/2\pi = 25$ Hz and $Q = 50$.

magnitude of the difference is defined by $(\phi_1 - \phi_0)/\phi_0$. Here ϕ_1 denotes the phase spectrum of the inverse operator for the dissipative medium and ϕ_0 denotes the phase spectrum of the inverse operator for the lossless medium. Three cases are illustrated in Fig. 3: (i) $\omega/2\pi = \omega_r/2\pi = 35$ Hz and $Q = 5$; (ii) $\omega/2\pi = \omega_r/2\pi = 35$ Hz and $Q = 50$; (iii) $\omega/2\pi = 35$ Hz, $\omega_r/2\pi = 25$ Hz and $Q = 50$.

The depth extrapolation scheme is performed by precalculating an operator table and then selecting the appropriate space-variant operator during the depth extrapolation process. From (4) we find that the value of $\omega^2/c^2(\omega)$ is determined by $\omega^{1-b}/c_0(\omega_r)$, where $b = (1/\pi)\arctan Q^{-1}$, and the quality factor Q (we assume ω_r is constant). Therefore the operator table should be constructed separately for different Q. This is done by first determining the maximum and minimum real phase velocities for the media that have the same Q, then calculating the short convolution operators for each value of ω^{1-b}/c_0 varying from $\omega_{\min}^{1-b}/(c_0)_{\max}$ to $\omega_{\max}^{1-b}/(c_0)_{\min}$ in a given interval based on the quality factor Q, and finally storing them in the part of the operator table corresponding to this Q. In this way, different gridpoints in the medium at different frequencies can use the same operator only if they have the same Q and if their ω^{1-b}/c_0 values are equal. A lossless medium can be considered as a medium with infinite Q. It can be seen that the operator table constructed here is easy to access during the depth extrapolation process.

IMAGING

There are two kinds of imaging conditions that can be used for imaging an anelastic medium. One is obtained by adapting that of the lossless case as

$$\Phi(\mathbf{x}) = \int \frac{P^{\mathrm{U}}(\mathbf{x},\omega)\{P^{\mathrm{D}}(\mathbf{x},\omega)\}^*}{P^{\mathrm{D}}(\mathbf{x},\omega)\{P^{\mathrm{D}}(\mathbf{x},\omega)\}^* + \varepsilon} \mathrm{d}\omega, \tag{19}$$

where $P^{\mathrm{D}}(\mathbf{x},\omega)$ is the one-way forward extrapolated downgoing source wavefield in the dissipative medium, $P^{\mathrm{U}}(\mathbf{x},\omega)$ the one-way inverse extrapolated upgoing receiver wavefield in the dissipative medium, and ε is a small stabilization constant. The other imaging condition is developed by designing a forward wavefield propagator in the adjoint effective medium that magnifies wavefields rather than attenuating them. Fortunately, this forward propagator can be easily obtained by taking the complex conjugate of the corresponding inverse propagator (see equation (14)). With $[P^{\mathrm{D}}(\mathbf{x},\omega)]'$ denoting the one-way forward extrapolated

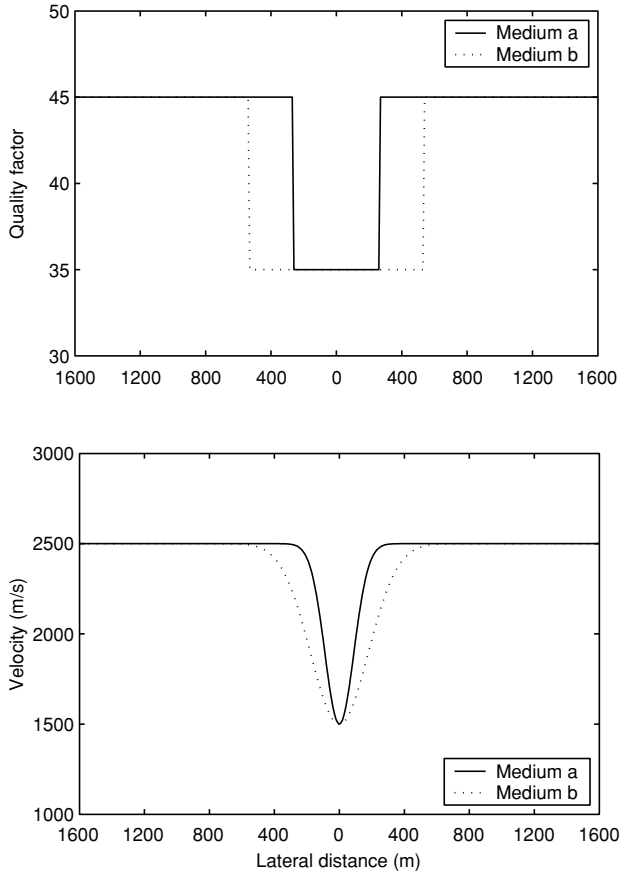

Figure 4 Lateral real phase velocity and quality factor profiles of two media a and b. The top figure shows the quality factor.

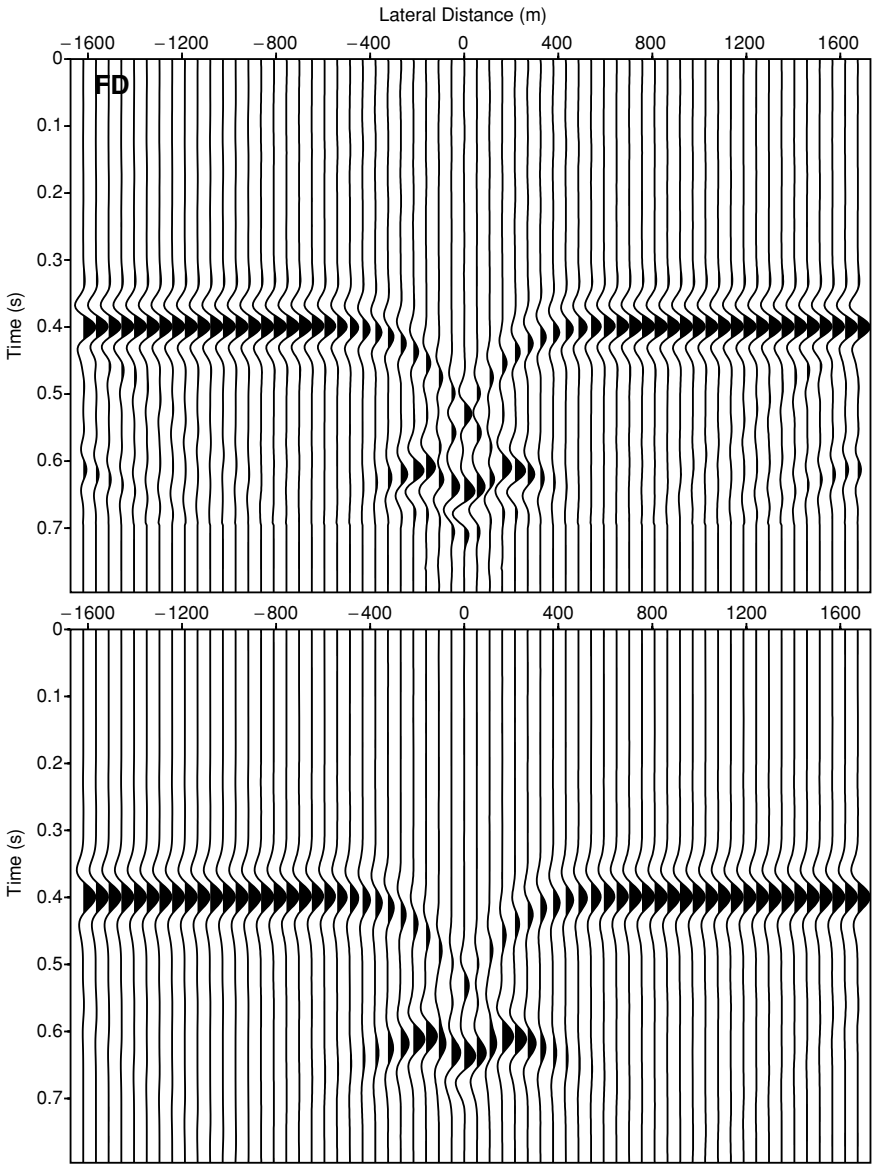

Figure 5 Comparison of the result of explicit depth extrapolation with that of finite-difference modelling of the two-way viscoacoustic equation for medium b. The top figure shows the finite-difference modelling result.

downgoing source wavefield in the adjoint effective medium, the second imaging condition can be expressed as

$$\Phi(\mathbf{x}) = \int P^{\mathrm{U}}(\mathbf{x}, \omega)\{[P^{\mathrm{D}}(\mathbf{x}, \omega)]'\}^{*}\mathrm{d}\omega. \tag{20}$$

The imaging condition of (20) was first proposed by Mittet *et al.* (1995) and was subsequently proved mathematically by Causse and Ursin (1999).

The imaging condition of (19) can give clearer deep imaging with little increase in noise in contrast to that of (20). Furthermore, the noise can be much reduced by common-depth-point stacking. However, for the imaging condition of (20), only one operator table, instead of two, needs to be constructed. This reduces the computational cost. In the following, we refer to (19) as the two-operator imaging condition, and to (20) as the one-operator imaging condition.

NUMERICAL EXAMPLES

Depth extrapolation

The proposed explicit depth extrapolation scheme is now compared with a frequency-domain finite-difference modelling of the two-way viscoacoustic equation. For this purpose

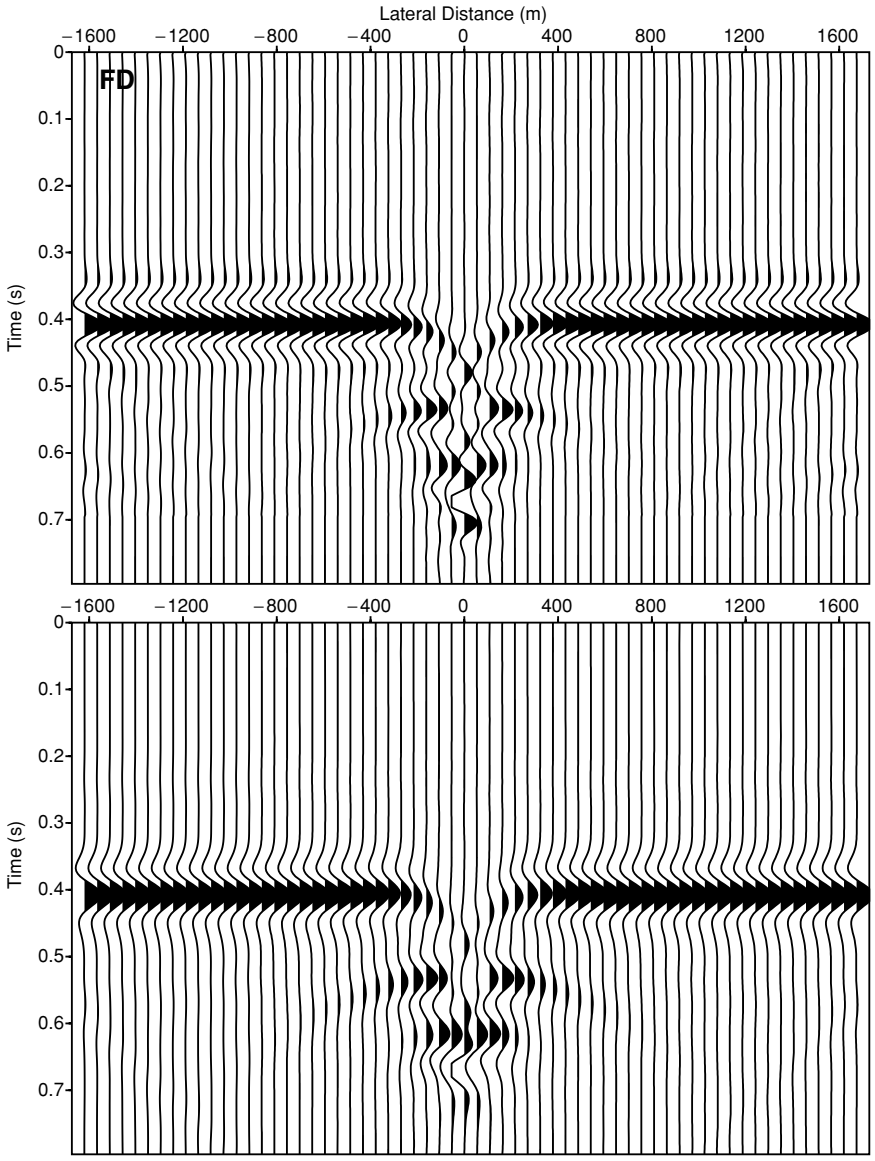

Figure 6 Comparison for a stronger lateral variation as in medium a. The top figure is the result of the finite-difference modelling, and the bottom figure is obtained by the explicit depth extrapolation.

we make use of media that are dependent only on the lateral coordinate. The lateral velocity (real phase velocity) and Q profiles of two media (a and b) are illustrated in Fig. 4. Medium a denotes a stronger laterally varying case, where the length of the disturbance is about three times the central wavelength. A vertically downgoing plane wave is introduced into the media. Recording takes place at a 1000-m depth level. The results of the numerical experiment in media a and b are shown in Figs 5 and 6. Although some numerical dispersion exists in the finite-difference modelling results due to a large discretized spatial sampling of $\Delta x = 9.0$ m, the two results agree well for both media a and b. This observation confirms that the proposed explicit depth extrapolation scheme is accurate for laterally varying dissipative media. Here the horizontal spacing for explicit extrapolation is $\Delta x = 27.0$ m, a 25-point explicit forward operator is used, and the wavelet contains frequencies up to 28 Hz. The difference in the positions of the peak of the wave curves for the flat parts in Figs 5 and 6 originates from the fact that we chose different reference frequencies for the two media. The reference frequency is $\omega_r/2\pi = 5.0$ Hz for Fig. 5 and $\omega_r/2\pi = 20.0$ Hz for Fig. 6. This experiment reveals that the absorption can influence the propagation velocity of the wavefront.

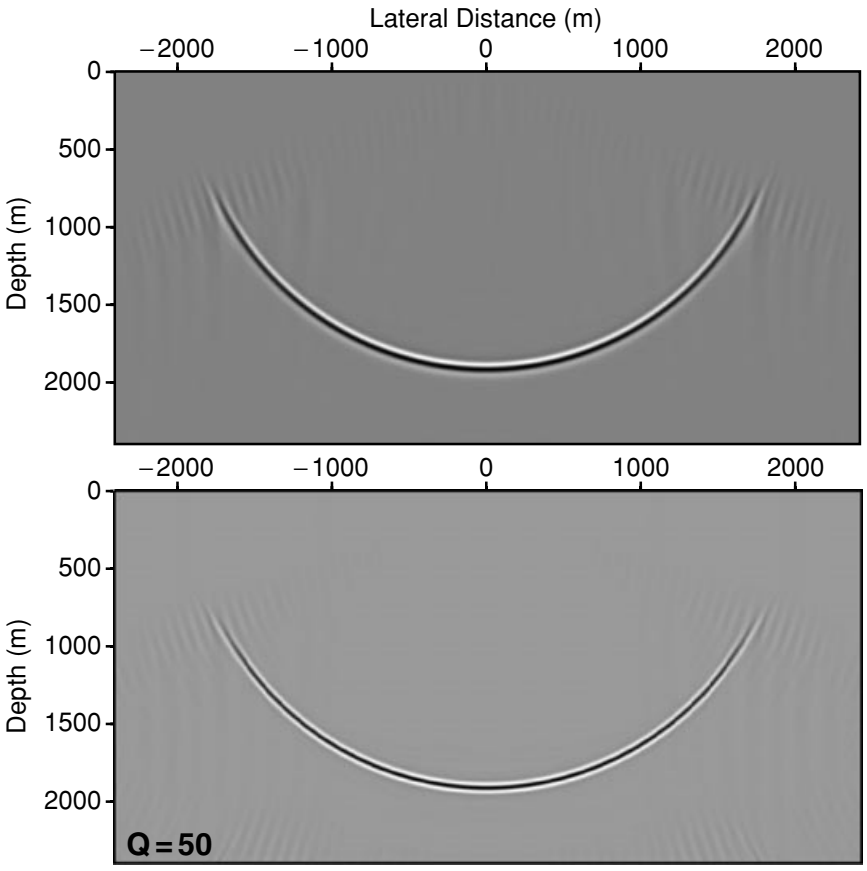

Figure 7 Comparison of migration impulse responses for a spatial impulse with dispersion. The top figure shows a result obtained for the acoustic case (i.e. no absorption compensation). The bottom figure is the result obtained by accounting for compensation for absorption. The maximum amplitude for the bottom figure is about 7.5 times that for the top figure. A 39-point explicit operator with a maximum angle of propagation of 57° is used.

Migration impulse response

The performance of the derived short explicit inverse operators is demonstrated by a study of migration impulse responses. For further testing of its compensation for absorption and dispersion, we design a spatial impulse by introducing dispersion to a Ricker wavelet, taking $Q = 50$. The wavelet contains frequencies up to 85 Hz. A 39-point explicit inverse operator with a maximum angle of propagation of 57° (due to stability) is used. Figure 7 compares the impulse response obtained with a real phase velocity of 2000 m/s and $Q = 50$ with that obtained under the acoustic assumption with $c_p = 2000$ m/s, i.e. neglecting compensation for attenuation and dispersion. The same spatial impulse is used for the two impulse responses. The maximum amplitude for the impulse response of $Q = 50$ is about 7.5 times that of the acoustic case. Figure 8 shows local detailed views of the comparison of the two impulse responses to illustrate the compensation for dispersion by the proposed explicit scheme. A total of 400 recursive applications of the explicit inverse operator from one depth level to the next, with depth steps of 6 m, are carried out. The good imaging quality demonstrates the effectiveness of the explicit extrapolation scheme.

Prestack depth migration

A synthetic seismic experiment is designed to test the proposed prestack migration scheme. The seismic data set is generated using a 2D frequency-domain finite-difference scheme of the two-way viscoacoustic equation. The subsurface velocity and Q models are shown in Fig. 9. In total, 46 shot records with shots moving from 828 m to 3258 m and a shot interval of 54 m are generated. A typical shot gather for the source positioned at 1800 m is shown in Fig. 10. To enhance the visibility of the figure, the data have been scaled with t^2. A sampling interval of $\Delta x = 9.0$ m is used in the modelling. For shot record migration, 25-point explicit operators with a maximum angle of propagation of 60° are designed. The horizontal spacing for migration is $\Delta x = 27.0$ m.

The common-depth-point stacked section using the two-operator imaging condition is shown in Fig. 11, which is

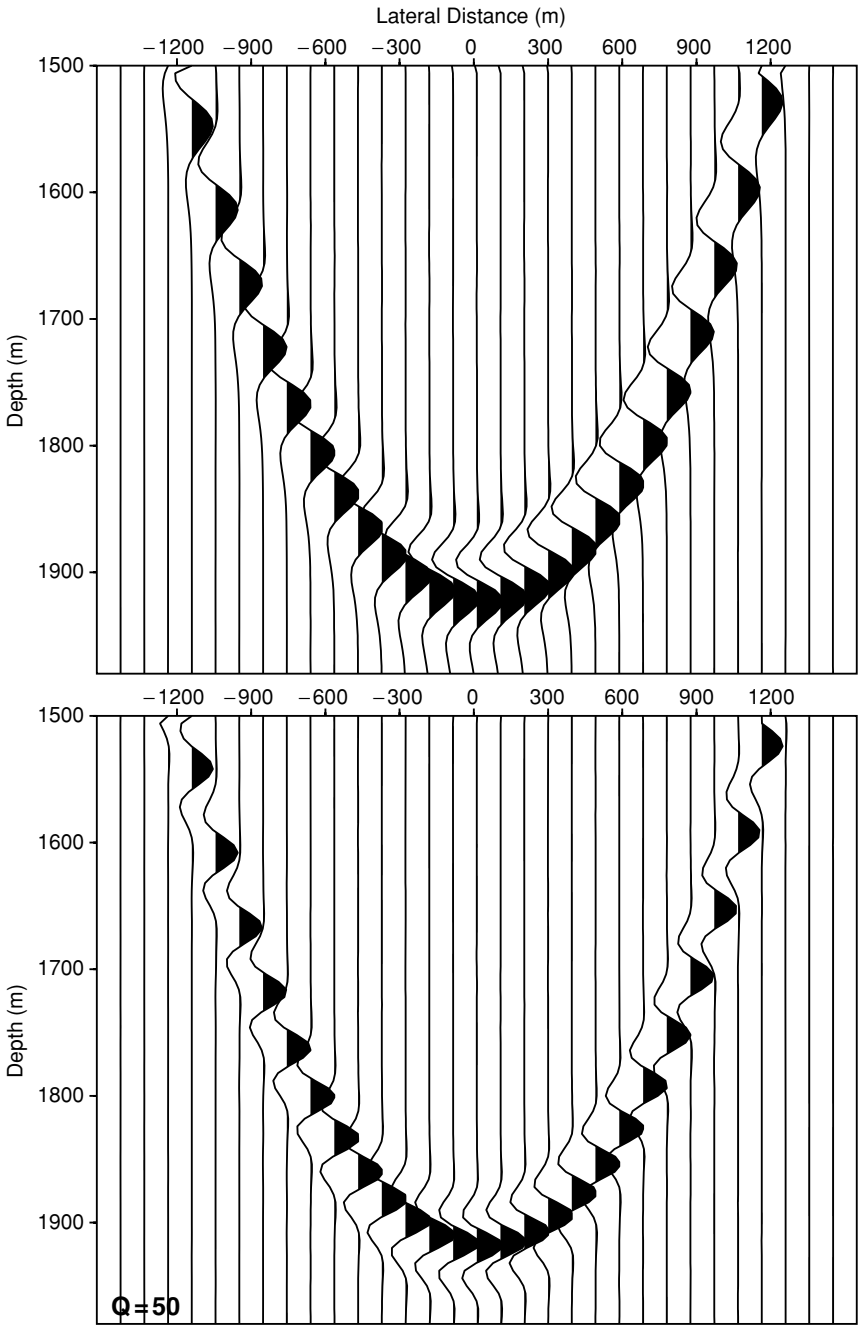

Figure 8 A local detailed view of Fig. 7.

constructed by superimposing the migrated section on the velocity model used in migration. From this figure we find that all reflectors are imaged and positioned at the correct locations. Moreover, the polarity reversal of the waveform, due to the fact that the wave is incident from a high velocity layer to a low velocity layer, is seen clearly at the location denoted by A. The results of Fig. 11 show that the proposed prestack migration scheme can image heterogeneous dissipative structures accurately.

A comparison of the migration result of the two-operator imaging condition with that of the one-operator imaging condition is shown in Fig. 12. It can be seen from this figure that the deep image is clearer using the two-operator imaging condition.

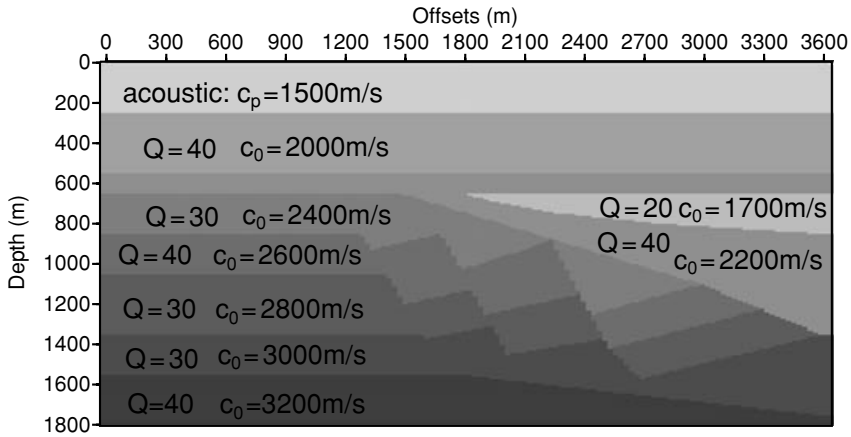

Figure 9 Subsurface real phase velocity and Q model.

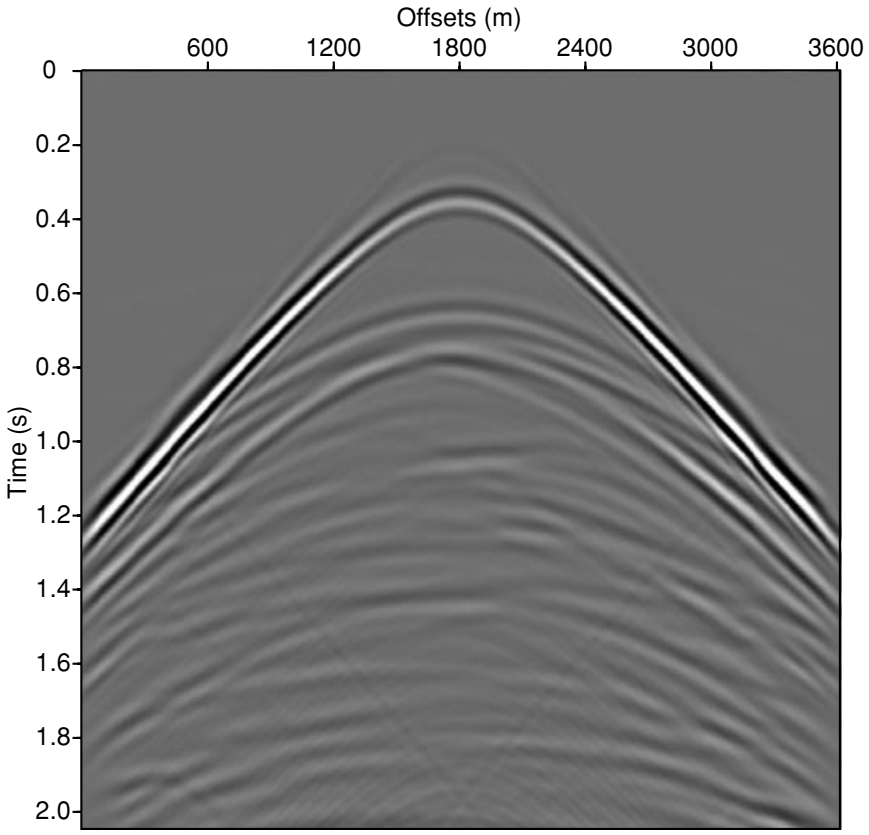

Figure 10 Shot gather for the source positioned at 1800 m. The shot gather is obtained using a frequency-domain finite-difference scheme. The data have been scaled with t^2 for display purposes.

A comparison with the acoustic migration result that takes no absorption into account (taking all Q in Fig. 9 to be positive infinite) is shown in Fig. 13. Both results are obtained using the two-operator imaging condition. The difference between them is distinct: the deep reflectors are imaged ambiguously with low amplitudes for acoustic imaging. This demonstrates the importance of including absorption in migration.

CONCLUSION

Methods for wavefield depth extrapolation and prestack imaging in complex anelastic media have been presented. The reciprocity theorem for one-way wavefields in dissipative media was applied to derive the inverse one-way propagator in inhomogeneous dissipative media. The resulting inverse propagator, which is stabilized by suppressing a part

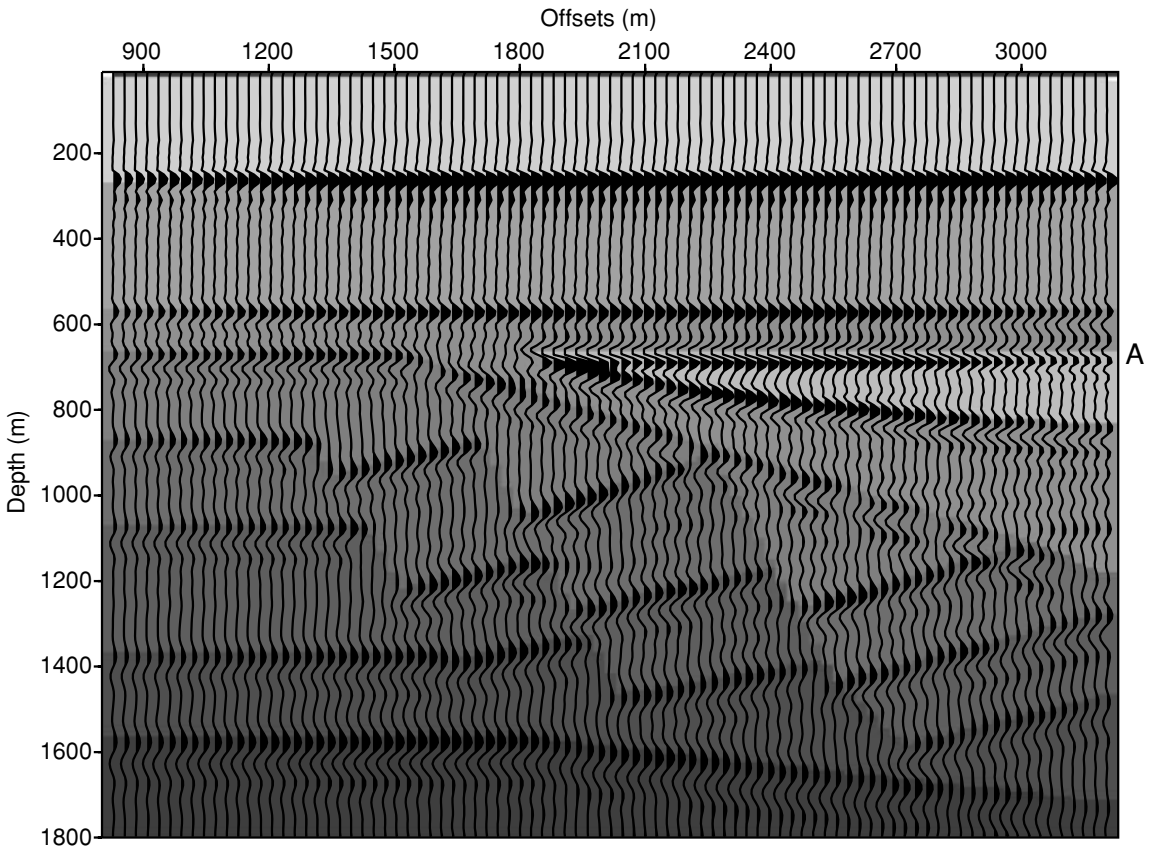

Figure 11 Prestack depth migration result obtained using the two-operator imaging condition. In total, 46 shot records with a shot interval of 54 m are applied. 25-point explicit operators with a maximum angle of propagation of 60° are used. The background is the velocity model used in migration.

of the eigenvalue spectrum of the associated square-root operator, can compensate well for attenuation and dispersion of seismic waves. Because of the need to limit the angle of propagation for stability, the explicit extrapolation operator scheme appears to be well suited for migration in inhomogeneous dissipative media. The macromodel we use is composed of a real phase velocity model, the same as the velocity model used in current migration schemes for lossless media, and an additional frequency-independent quality factor macromodel. The proposed explicit scheme is performed by precalculating an operator table and then selecting the space-variant convolution operator at each gridpoint according to the real phase velocity and quality factor at this gridpoint and the temporal frequency during the depth-extrapolation process. The absorption effects influence only the design of the convolution operators. Hence, the resulting algorithm can easily be incorporated in existing migration schemes. The short convolution operators are designed by adapting the weighted least-squares method, which can derive a highly accurate short operator at a very low computational cost.

The accuracy of the proposed explicit depth extrapolation scheme was demonstrated by comparing the results of the explicit depth extrapolation with those of the finite-difference method for modelling the transmission response of a laterally varying medium. The potential of the derived explicit inverse operators was further illustrated by the migration impulse response of a spatial impulse with dispersion. Finally, a synthetic data set, obtained by a finite-difference method based on the two-way viscoacoustic wave equation, was used to test the proposed prestack depth migration scheme. The numerical example shows a significant improvement in the images when migrating with compensation for absorption, as compared with images obtained by neglecting the absorption.

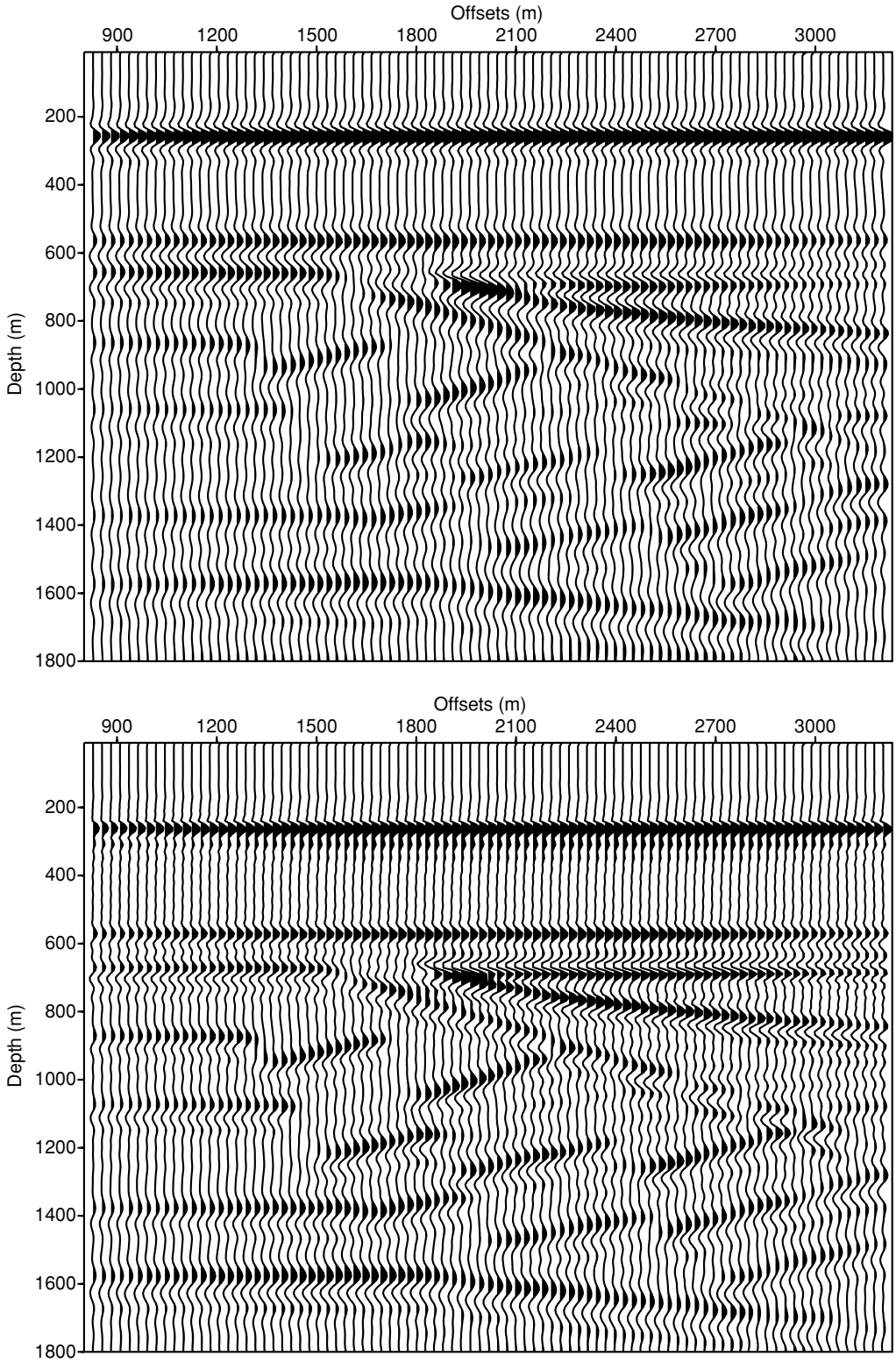

Figure 12 Comparison of the prestack depth migration result of the two-operator imaging condition with that of the one-operator imaging condition. The top figure shows the result of the one-operator imaging condition.

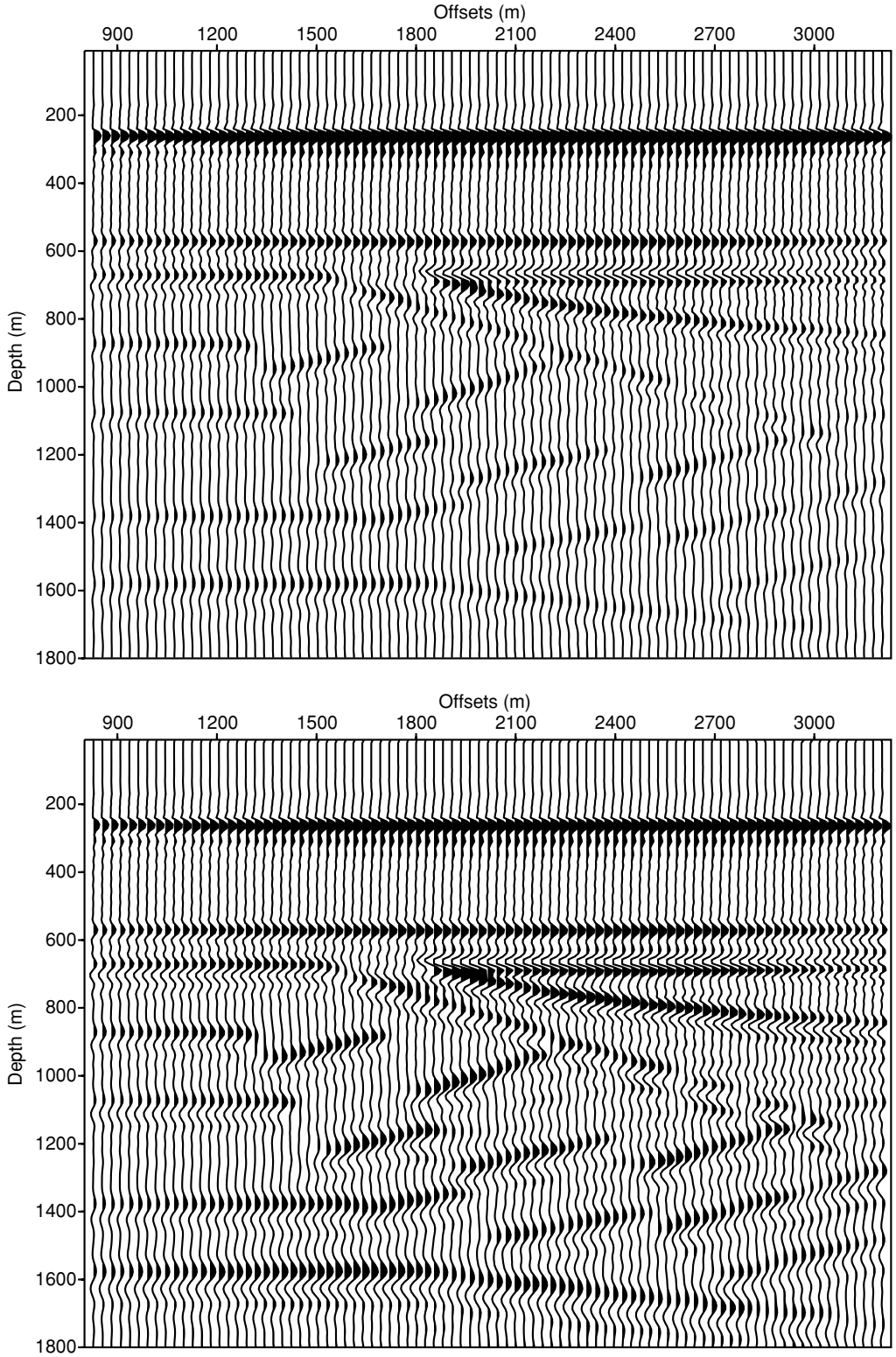

Figure 13 Comparison of the prestack depth migration results with and without compensation for absorption. The top figure shows the prestack depth migration result obtained without compensation for absorption, that is, the velocity model of Fig. 9 is used but the quality factors are assumed to be infinite. The two-operator imaging condition was used for obtaining both results.

ACKNOWLEDGEMENT

J.Z. thanks the Netherlands Research Centre for Integrated Solid Earth Science for supporting his research fellowship at Delft University of Technology.

REFERENCES

Aki K. and Richards P.G. 1980. *Quantitative Seismology*. W.H. Freeman.

Amundsen L. and Mittet R. 1994. Estimation of phase velocities and Q-factors from zero-offset vertical seismic profile data. *Geophysics* **59,** 500–517.

Carcione J.M., Kosloff D. and Kosloff R. 1988. Wave propagation simulation in a linear viscoelastic medium. *Geophysical Journal* **95,** 597–611.

Causse E. and Ursin B. 1999. Asymptotic error analysis of constant-velocity viscoacoustic migration. *Geophysics* **64,** 1036–1045.

Causse E. and Ursin B. 2000. Viscoacoustic reverse-time migration. *Journal of Seismic Exploration* **9,** 165–184.

Emmerich H. and Korn M. 1987. Incorporation of attenuation into time-domain computations of seismic wavefields. *Geophysics* **52,** 1252–1264.

Etgen J. 1994. Stability of explicit depth extrapolation through laterally varying media. 64th SEG meeting, Los Angeles, USA, Expanded Abstracts, 1266–1269.

Grimbergen J.L.T., Dessing F.J. and Wapenaar C.P.A. 1998. Modal expansion of one-way operators in laterally varying media. *Geophysics* **63,** 995–1005.

Hale D. 1991. Stable explicit depth extrapolation of seismic wavefields. *Geophysics* **56,** 1770–1777.

Holberg O. 1988. Toward optimum one-way wave propagation. *Geophysical Prospecting* **36,** 99–114.

Keers H., Vasco D.W. and Johnson L.R. 2001. Viscoacoustic cross-well imaging using asymptotic waveforms. *Geophysics* **66,** 861–870.

Kjartansson E. 1979. Constant Q wave propagation and attenuation. *Journal of Geophysical Research* **84,** 4737–4748.

Mittet R., Sollie R. and Hokstad K. 1995. Prestack depth migration with compensation for absorption and dispersion. *Geophysics* **60,** 1485–1494.

Robinson J.G. 1979. A technique for the continuous representation of dispersion in seismic data. *Geophysics* **44,** 1345–1351.

Soubaras R. 1996. Explicit 3-D migration using equiripple polynomial expansion and Laplacian synthesis. *Geophysics* **61,** 1386–1393.

Stekl I. and Pratt R.G. 1998. Accurate viscoelastic modeling by frequency-domain finite differences using rotated operators. *Geophysics* **63,** 1779–1794.

Thorbecke J.T. and Rietveld W.E.A. 1994. Optimum extrapolation operators: a comparison. 56th EAGE meeting, Vienna, Austria, Extended Abstracts, P105.

Wapenaar C.P.A. and Berkhout A.J. 1989. *Elastic Wave Field Extrapolation*. Elsevier Science Publishing Co.

Wapenaar C.P.A., Dillen M.W.P. and Fokkema J.T. 2001. Reciprocity theorems for electromagnetic or acoustic one-way wave fields in dissipative inhomogeneous media. *Radio Science* **36,** 851–863.

Zhang J., Verschuur D.J. and Wapenaar C.P.A. 2001. Depth migration of shot records in heterogeneous, transversely isotropic media using optimum explicit operators. *Geophysical Prospecting* **49,** 287–299.